Mechanics of the Selective Laser Raster-Scanning Surface Interaction

J.A. Ramos[1], D.L. Bourell[2]

(1) Department of Mechanical and Metallurgical Engineering, Pontificia Universidad
Católica de Chile, Vicuña Mackenna 4860, Santiago, Chile
(2) Department of Mechanical Engineering, Laboratory for Freeform Fabrication   The
University of Texas at Austin, Austin, Texas, 78712

ABSTRACT

In recent years, the use of a high power laser beam actuated by fast speed scanning mirrors has opened up novel selective laser raster-scan processing venues as extremely rapid motion and high overlapping of the beam can be attained. This permits distribution of laser energy precisely over geometric patterns such as rectangles, circles, triangles etc. The surface thermal history at any given point under such processing was estimated using an analytical solution for the 1D, semi-infinite, surface flux boundary condition heat conduction problem together with linear superposition theory. Presented here is the comparison of the thermal histories of different selective laser surface processes previously implemented, namely: laser surface polishing of flat surfaces, laser induced cementation of cylindrical surfaces and direct laser single layer masked deposition. It was possible to verify that in laser induced cementation, long-width and short-length scanned regions provided low average temperature and low heating rate with spaced out temperature peaks, whereas for direct laser single layer deposition in which a narrow-width – long-length region is scanned, the heating rate and peak temperature are higher and the peaks are squeezed. The analysis also provided ways to estimate the Andrew's number associated with a raster-scan process for the sake of comparison with single-beam processes having a given number value. Understanding the influence of scan geometry and overlapping on the selective raster-scan processing provides a method to tailor the surface peak temperature as well as the heating and cooling rates, affecting the solidification or sintering conditions and therefore the mechanical properties of the parts obtained.

Introduction

It was in the mid 80s when the need to deposit low power infrared laser energy selectively in space over the surface of materials became a necessity for the development of certain rapid prototyping technologies that were evolving at that time. One particular case, was the development of the Selective Laser Sintering (SLS) process created at the University of Texas at Austin [1]. Energy deposition in 2D space was achieved by modulating laser energy using galvanometer driven mirrors. The main advantage of the "galvo-mirrors" was the fact the laser beam could be raster-scanned at much higher

speeds, along any planar trajectory, than any conventional positioning mechanism available then such as CNC x-y tables.

By raster-scanning a focused laser beam along a zig-zag pattern, galvanometer driven mirrors allowed the creation of a "pseudo-energy-line" source capable of sustaining an homogenous melting front of certain width. The traveling speed, V_t, (slow-direction) of this front is a function of the scan speed, V_s, (fast direction) and the density of scanning lines. The latter in turn, determined the percent of scanning-line overlap, ϕ, for a given beam spot diameter size. However, it was not until early 90s that high-laser-power handling galvo-mirror delivery systems became available to investigators. By 1998 Das *et al.* at the University of Texas at Austin had built two such SLS stations capable of harnessing up to 1.4 kW from a CO_2 laser and 500 W from a Nd:YAG for research purposes [2].

In this work the thermal history at any surface point under laser raster-scan processing was estimated numerically using the analytical solution to the 1D, semi-infinite, surface flux boundary condition heat conduction problem together with linear superposition theory. Results were obtained for the thermal histories of different laser surface processes, namely: laser surface polishing of a planar surface, laser induced cementation of a cylindrical surfaces and direct laser single layer masked deposition. Common variables to all these processes are: width and length of the scanned rectangular region, number of scanning lines, scan speed along the width and laser power.

Laser Surface Polishing of Indirect-SLS Parts

Laser surface processing is emerging as a suitable technique for reducing surface roughness in metals, ceramics and polymer materials as it offers several modification regimes depending on the laser processing parameters. [3-5]. The schematic drawing of the laser polishing process utilized to reduce the surface roughness of indirect SLS parts is illustrated in Figure 1 [7].
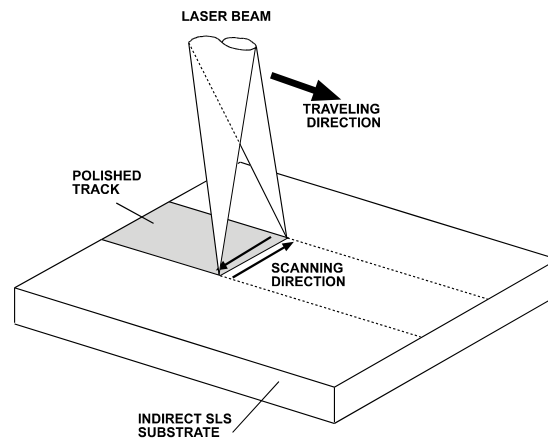

Figure 1. Schematic diagram of the laser polishing process.

A focused laser beam of sufficient power to shallowly melt the surface of the object was raster-scanned at high speed a long a rectangular track. The length to width aspect ratio of the scan track in this case ranged from 5 to 12.5; a geometric file with 2000 scanning lines/inch was used.

Laser Induced Cementation of Cylindrical Substrates

The purpose is to develop a laser fusion methodology to deposit coatings over cylindrical ceramic substrates. The scanning trajectory of the focused laser beam is programmed so that the beam scans back and forth along the major axis of the cylinder a narrow fringe with a small length to width aspect ratio of 0.05 using up to 4000 scanning lines/inch. The laser beam was scanned over the specimen the same amount of time the cylindrical specimen was rotated. Figure 2 illustrates the set up developed to carry out the laser induced cementation process [7]. The cylindrical specimen rotates suspended from a narrow stem while the focused laser beam raster-scans back and forth a long the longitudinal length of the cylinder.
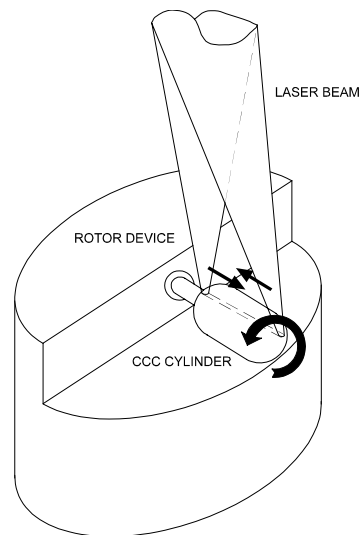

Figure 2. Schematic drawing of the "Laser Induced Cementation" process.

Direct Laser Single Layer Masked Deposition

Finally, in this research the objective is to restore superalloy single crystal components (e.g. aircraft combustion engine turbine blades) to near original properties and dimensions. It is crucial to develop the ability to tailor the microstructure of the deposited material as it is being laid. A schematic diagram of the laser melting process used in this work is illustrated in Figure 3 [7]. The laser beam raster-scans back and forth laterally and travels along the mask trough, melting the entire powder depth and a small fraction of the substrate. As the melt pool advances its tail solidifies forming a sound metallurgical bonding with the substrate. The length to width aspect ratio of the scan

track in this case corresponds to 12.5 and a total of 7000 scanning lines/inch is considered.
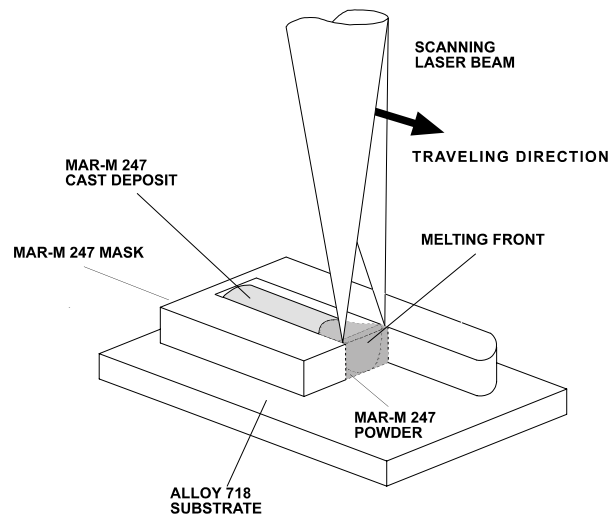

Figure 3. Overall schematic of the mask-powder-substrate arrangement during selective laser melting.

Mechanics of a Raster-Scanned Laser Beam

In recent years, the use of high-power laser beams actuated by high-speed scanning mirrors has opened up novel surface raster-scan processing venues as extremely rapid motion of the beam (> 0.5 m/s in the scan direction) and high percentage overlap (> 99.9%) can be attained. This permits distribution precisely of laser energy along specific geometric patterns such rectangles, circles, triangles or almost any complex closed regions. Because of this processing scheme, each point at the surface of the material experiences multiple high-frequency heating-cooling (HC) cycles during the overall laser scanning time. The HC cycle period is a function of position along the scanning direction and overall geometry of the scanning pattern.

Energy Density Relationship: Raster-Scan and Line Sources

The Andrew's number (Eq. 1) is a measure of the energy deposited per unit area over the surface of a material by a moving energy source. It can also be expressed as the power deposited over an area that is being continuously displaced per unit time; thus for a given laser power, P, focused at a spot of diameter, D, which moves with a traveling speed, V_t, the Andrew's number becomes,

$$A_{SPOT} = \frac{P}{D \cdot V_t} \qquad (1)$$

If the energy source were no longer circular but of rectangular shape, with dimensions D and W, where W corresponds to the width of the source and D the thickness; in the case of W>>D, the source can be considered a line source having its speed, V_L, perpendicular to its width, W. The Andrew's number then becomes

$$A_{LINE} = \frac{P}{W \cdot V_L} \qquad (2)$$

If such linear source moved a length L, then the overall rastered area would be L*W. The average time taken to cover that area is, $\Delta t = \dfrac{L}{V_L}$, and the total energy density deposited corresponds to, $\dfrac{P \cdot \Delta t}{L \cdot W}$. Therefore, Eq. 2 is verified, when Δt is substituted in. Now let us consider what happens when the area, L*W, is rastered not by a line source of width W, but by a spot source of diameter, D, that scans parallel to the width W of the area. Figure 4 shows a schematic illustration of this laser raster scan process.
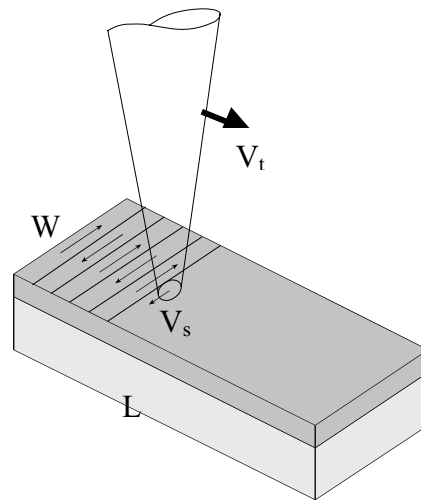

Figure 4. Schematic of a typical laser raster-scan fusion coating process.

Moreover, it is assumed that there is not overlap of the spot source as it travels back and forth the width W at a speed V_s (generally faster than the traveling speed V_t), so that at each edge, its perpendicular position is offset a distance D. Then, the number of scan-lines required to cover the area L*W becomes,

$$N = \frac{L}{D} \qquad (3)$$

In this situation the average time taken to cover the raster-scanned area, L*W, can be expressed as,

$$\Delta t_{R-S} = \frac{N \cdot W}{V_S} = \frac{L \cdot W}{D \cdot V_S} \qquad (4)$$

and the total energy deposited over the area, L*W, by the raster-scanned source now becomes,

$$\frac{P \cdot \Delta t_{R-S}}{L \cdot W} = A_{R-S} = \frac{P}{D \cdot V_S} \qquad (5)$$

We can then conclude that in order to obtain the same Andrew's number associated with the area, L*W, and a fixed laser power, P, the following equivalence relation (from Eq. 2 and 5) must hold:

$$\frac{V_L}{V_S} = \frac{D}{W} \qquad (6)$$

That is, the equivalence between the traveling speed, V_L, of a line source of width W, relates to the raster-scan speed, V_S, of a spot source of diameter D, by the quotient, D/W, which is generally less than 1.

If we now allow a certain amount of overlapping between successive scanned lines, we may define the percentage of overlap, ϕ, as,

$$\phi = 1 - \frac{\Delta x}{D} \qquad (7)$$

Where, Δx, is the distance between the corresponding edges of two successive scanned tracks as illustrated in Figure 5 .
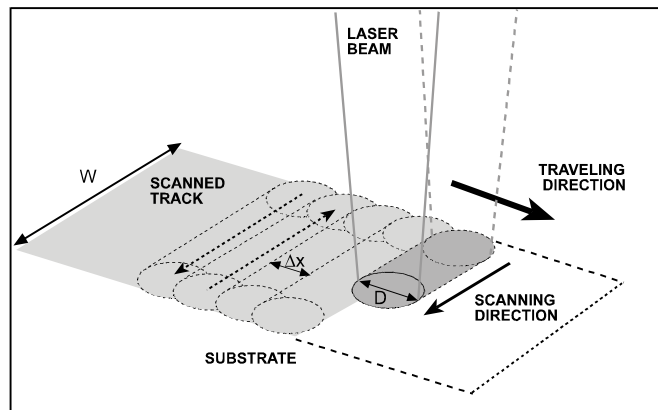

Figure 5. Schematic illustration of the overlapping of raster scans tracks.

Then, the number of scan lines, N_{OL}, when overlap exists, needed to cover the area, L*W, becomes,

$$N_{OL} = \frac{L}{(1-\phi)\cdot D} \tag{8}$$

The average time taken to cover such an area is,

$$\Delta t_{R\text{-}S/OL} = \frac{L\cdot W}{(1-\phi)\cdot D\cdot V_S} \tag{9}$$

and the total energy deposited over L*W by the raster-scanned and overlapped source is,

$$\frac{P\cdot\Delta t_{R\text{-}S/OL}}{L\cdot W} = A_{R\text{-}S/OL} = \frac{P}{(1-\phi)\cdot D\cdot V_S} \tag{10}$$

The equivalence relationship then becomes,

$$\frac{V_L}{V_S} = \frac{D}{W}\cdot(1-\phi) \tag{11}$$

This relationship verifies Eq. 5 when $\phi = 0$, i.e., when no overlap exists. Simultaneously, when ϕ is non-zero, the average traveling speed, V_t, of the raster-scanned source becomes,

$$V_t = \frac{L}{\Delta t_{R\text{-}S/OL}} = (1-\phi)\cdot\frac{D}{W}\cdot V_s \tag{12}$$

It can be observed that Eq.12 is equivalent to Eq. 11. This means that when Eq. 11 holds, the traveling speed of the line source, V_L, corresponds to the average traveling speed of the raster-scanned source.

Surface Temperature Evolution During Laser Raster-Scanning

At a given point on the surface, the temperature increase due to the heating portion of the heating-cooling cycle can be modeled through the analytical solution to the 1-D, semi-infinite, flux boundary heat conduction problem. The core of the heat conduction problem is the known parabolic differential equation in one-dimensional space,

$$\frac{\partial^2 T}{\partial z^2} = \frac{1}{\alpha} \cdot \frac{\partial T}{\partial t} \tag{13}$$

with initial temperature, T_o, over all the domain, and at the surface of the specimen, the flux boundary condition is,

$$K \cdot \frac{dT}{dz}\bigg|_{z=0} = I \tag{14}$$

where, I, is the power density of the laser beam,

$$I = \frac{(1-\mathfrak{R}) \cdot P}{A} \tag{15}$$

$\mathfrak{R}$ incorporates the effect of surface reflectivity, which is a strong function of the laser wavelength, as well as radiative and convective surface heat losses. The area illuminated by the beam, A, can be circular as in the case of a raster-scanned-source (i.e., $\pi \cdot D^2/4$) or rectangular as for a line-source (i.e., $W \cdot D$).

The analytical solution to this problem provides a uniaxial temperature distribution in closed-form, which is a function of position and time in the semi-infinite solid [3,6],

$$T(z,t) = \frac{2 \cdot I}{K} \cdot \left(e^{-\frac{z^2}{4 \cdot \alpha \cdot t}} \left(\frac{\alpha \cdot t}{\pi} \right)^{0.5} - \frac{z}{2} \cdot \mathrm{erfc} \left(\frac{z}{(4 \cdot \alpha \cdot t)^{0.5}} \right) \right) \tag{16}$$

Here, α and K correspond to the thermal diffusivity and heat conductivity of the solid respectively, and erfc( ) is the complementary error function. When evaluated at $z = 0$, Eq. 16 then simplifies down to

$$T(z,t)\big|_{z=0} = T(t) = \frac{I}{K} \cdot \left(\frac{4 \cdot \alpha \cdot t}{\pi} \right)^{0.5} \tag{17}$$

Linear superposition theory can then be applied to obtain both the heating and the cooling portion of the HC cycle [3,6]. The latter, after the heat source has stopped interacting for a given time interval, D/V_s, is approximately equivalent of being turned off. This corresponds to the following surface boundary condition,

$$K \cdot \frac{dT}{dz}\bigg|_{z=0} = \begin{cases} I \text{ for } 0 < t \leq \dfrac{D}{V_S} \\ 0 \text{ for } t > \dfrac{D}{V_S} \end{cases} \qquad (18)$$

The resulting expression for the complete temperature evolution has the form,

$$T_{HC}(t, \tau_0) = T(t) \cdot H(t) - T(t-\tau_0) \cdot H(t-\tau_0) \qquad (19)$$

where H(t), corresponds to the Heaviside step function and τ_0 is half the laser interaction time interval or heating time, $D/2V_s$. This is the time one half the laser spot spends traveling over a specific surface coordinate. This time interval causes increase in local surface temperature and corresponds to the first term on the right hand side of Eq. 19. The heating cycle is immediately followed by a cooling cycle that corresponds to the second term on the right hand side of Eq. 19. The complete HC cycle is illustrated in Figure 6.
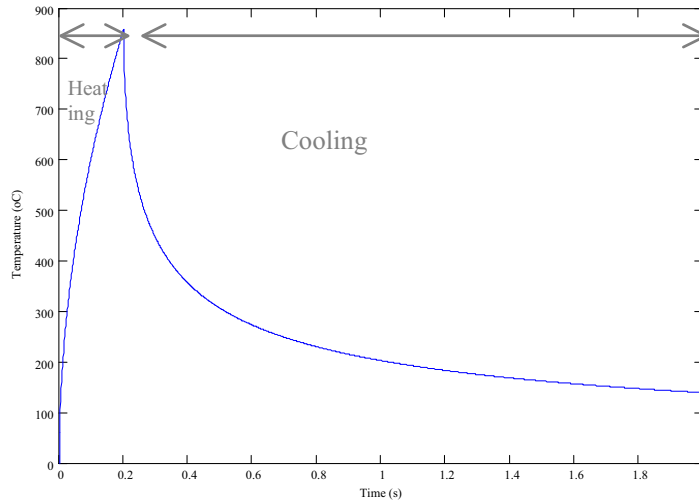

Figure 6. Typical heating cycle followed by the corresponding cooling cycle after the source is turned off or displaced.

Linear superposition theory can be further applied to determine the superposition of temperature histories due to multiple overlaps. An arbitrary x position, along the scan-width W is considered, measured from the left edge. The temperature evolution at this location during the initial heating interval at each complete raster scan cycle, is determined then by,

$$f_{\text{Initial}}(t, \tau_1, \tau_2) = \sum_{i=0}^{\frac{1}{1-\phi}} \left(1 - (1-\phi) \cdot i\right) \cdot \left[T(t-\tau_1) \cdot H(t-\tau_1) - T(t-\tau_2) \cdot H(t-\tau_2) \right] \qquad (20)$$

567

Where the summation limit, $1/1-\phi$, refers to the number of times the laser has to scan over its spot area in order to raster it completely. After every scan, the beam is offset a percentage, $1-\phi$, of the total spot width, so the intensity of the heat flux experienced by the space coordinate, x, is assumed to decay as $1-(1-\phi)*i$, where, i, is the summation index corresponding to the raster-scan number count. Here, τ_1, corresponds to one full raster scan time interval in which the source travels from the x coordinate and back to it, and, τ_2, corresponds to the same interval plus a heating cycle of length D/2.

Additionally, the temperature evolution during first cooling interval (the time it takes the source to travel from the x coordinate to the right edge of the width and then back to the former) is given by a similar relationship,

$$f_{\text{Right}}(t,\tau_3,\tau_4) = \sum_{i=0}^{\frac{1}{1-\phi}} \left(1-(1-\phi)\cdot i\right)\cdot\left[T(t-\tau_3)\cdot H(t-\tau_3) - T(t-\tau_4)\cdot H(t-\tau_4)\right] \qquad (21)$$

However, here the function τ_3, corresponds to the cooling interval as the beam moves away from x to W and from W to back x, and the function τ_4, corresponds to the same cooling interval plus one heating cycle of length: D when $0 < x < W$, D/2 when x = 0, and zero heating interval when x = W.   Similarly, the temperature evolution during the second cooling interval (this is time it takes the source to travel from x to the left edge of the width, and then back to the former) is given once again by,

$$f_{\text{Left}}(t,\tau_5,\tau_6) = \sum_{i=0}^{\frac{1}{1-\phi}} \left(1-(1-\phi)\cdot i\right)\cdot\left[T(t-\tau_5)\cdot H(t-\tau_5) - T(t-\tau_6)\cdot H(t-\tau_6)\right] \qquad (22)$$

This differs only in the form of the cooling intervals, τ_5 and τ_6. Thus, the temperature profile at a given position, x, for a raster scan processing, as a function of time is, given by the sum of the latter three expressions:

$$T(t,x)_{\text{Raster-Scan}} = f(t,\tau_1,\tau_2)_{\text{Initial}} + f(t,\tau_3,\tau_4)_{\text{Right}} + f(t,\tau_5,\tau_6)_{\text{Left}} \qquad (23)$$

More details on this model can be found in Ref. 7.

To illustrate the use of Eq. 23, a plot of a typical sequence of heating and cooling cycles when two complete back and forth raster scans are performed is presented in Figure 7. The continuous line corresponds to the temperature measured at the center of the width while the dotted line corresponds to the temperature as measured at either one of the edges. In the both cases, the first and last peaks are narrower as it corresponds to half the total heating interval, $D/2V_s$, whereas the other peaks correspond to a full heating interval.
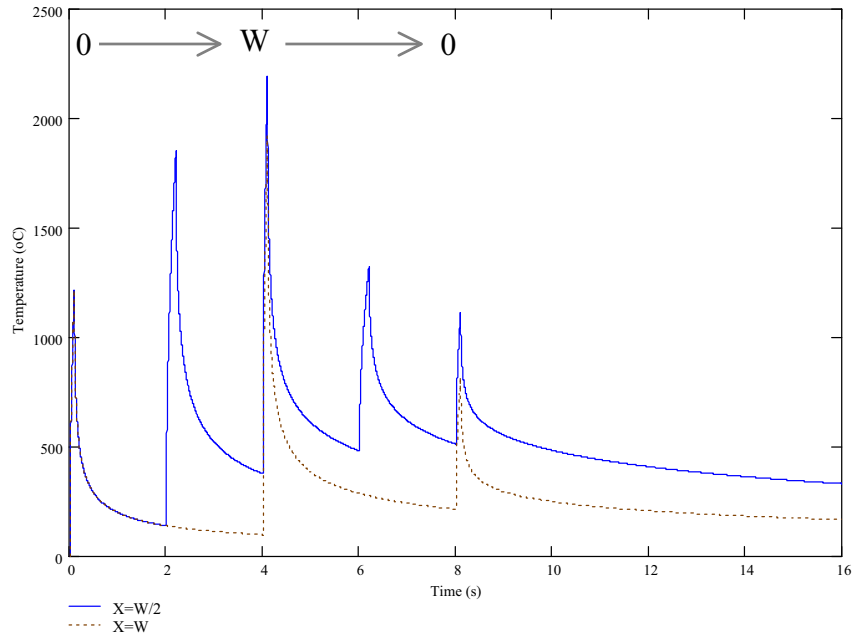
Figure 7. Typical sequence of heating and cooling cycle when a complete back and forth raster scan is performed.

Simulation Results and Discussion

Numerical implementation of Eq. 23 was done and the temperature profile results are plotted in Figure 8. These temperature profiles were evaluated at half the width of the scan pattern. These results were used to compare the thermal histories of three different laser surface processes, namely: (a) laser surface polishing of flat surfaces, (b) laser induced cementation of cylindrical surfaces and (c) direct laser single layer masked deposition. However, to compare the different temperature profiles, the material properties, the laser power and spot diameter on all three processes were equally assigned. Temperature independent materials properties for 420 stainless steel-40wt.% bronze alloy were considered, the laser power was set equal to 250 W, and the spot size was 0.4 mm. Variables common to all these processes were: width, W, and length, L, of the scanned rectangular region, number of scanning lines, N, and the overall scanning time, Δt, These variables were assigned different values for each of the three processes as illustrated in Table 1. The percent overlap, f, the scan speed, the Andrew's number and the traveling speed were calculated from Eq. 8,9,10 and 11, respectively.

Table 1. Processing variables for three difference laser raster-scan process.

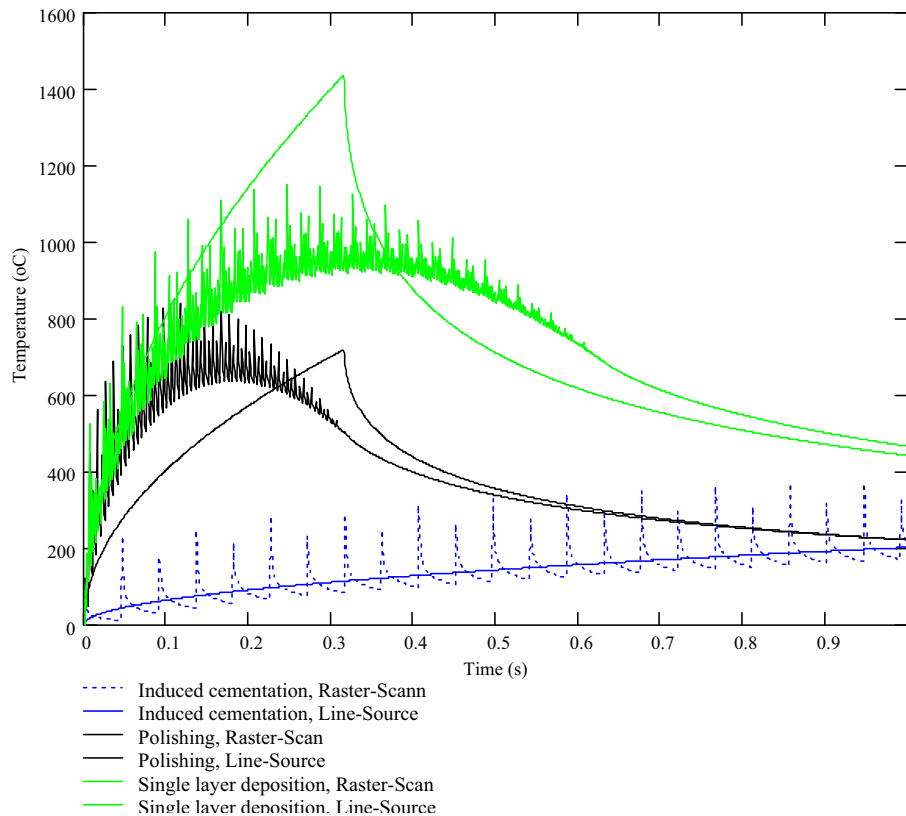| Process	L (mm)	W (mm)	Δt (s)	N (line/inch)	ϕ (%)	V_s (mm/s)	$A_{R-S/OL}=A_L$ (J/mm²)	$V_t = V_L$ (mm/s)
a	25.4	4	20	2000	96.825	400	49.21	1.27
b	1.3	25.4	180	4000	99.919	564.4	1367.1	0.0072
c	25.4	2	20	7000	99.093	700	98.44	1.27

Figure 8. Surface temperatures at a fixed position versus interaction time for raster-scan processing and line-source processing for 3 different processes.

From Figure 8 it can be observed that for a diffusion-driven process like the laser induced cementation, long-width short-length scanned regions (L/W = 0.32) with intermediate number of scan lines (N=4000), provide a low average temperature with spaced out sharp temperature peaks, whereas for narrow-width long-length scanned regions (L/W = 6.35) with lower number of scan lines (N=2000) as in the case of laser polishing, the average temperature is higher but short lived, and the temperature peaks are shorter and much closer together. When increasing the number of scan lines (N=7000) and doubling the length to width ratio (L/W= 12.7) as in direct laser single layer masked deposition, the average temperature is higher than in the previous case and it also lasts longer and the peak temperatures are less spaced out than in the first case.

The temperature history obtained for a line source of equal power and traveling speed, along the length direction, is also plotted in Figure 8 for comparison purposes from a single heating-cooling cycle as given by Eq. 19. In the case of processes (a) and (c), the temperature profile shows the same heating interval length because of the same traveling speed (1.27 mm/s), but for the former the peak temperature is lower as the associated Andrew's number (44.22 J/mm^2) is half that of the latter (98.44 J/mm^2). This

is because of the twofold difference in number of scan lines (2000 versus 4000 lines/inch). In the case of the laser polishing process, the peak average temperature obtained by the raster-scan and the line sources are very close in magnitude. However, the heating interval for the raster-scan is almost half that of the line source due to the lower percent overlap (96.83%). The heating rate is also steeper for the raster-scan source than for the line source, while the cooling rate is steeper for the line source only at the beginning of the cooling cycle. In the case of process (c), a much higher peak temperature is obtained with the line-source as well as steeper heating and cooling rates. Moreover, the peak average temperature of the raster-scan source occurs at almost the same heating interval as the peak temperature of the line source due to the high percentage overlap (99.09%). In the case of process (b), the corresponding Andrew's number is the highest of the three processes (1367 J/mm^2). However, it can be observed that the line source temperature is not much higher than the mean temperature obtained for a raster-scan source, and the peak temperatures from the latter source are higher in this particular case. The maximum average temperature is achieved for the longest heating interval of the three processes due to the largest percentage overlap used (99.92%).

It is worth noting that for all three processes, the Andrew's numbers of the line and raster-scan sources are the same as imposed by the equivalence relationship given by Eq. 11.

Conclusions

Equation 11 is a general and useful relationship that allows to comparison of surfaces that have been laser processed and thus modified by line or raster scanned sources, keeping constant in both cases the Andrew's number by varying ϕ and Vs, when W, L, D and V_t are kept constant.

Increasing the number of scan lines (N) while keeping constant the traveling speed ($V_L=V_t$) and laser power (P) produces higher peak temperatures after heating intervals that approach the limiting value given by a (D/V_L) for a line source traveling at the same speed. This is because the percent overlap, ϕ, is increased towards 1.

For a fixed traveling speed, increasing the number of scan lines increases the scan speed provided the length to width aspect ratio is kept constant as determined by Equation 11.

If the number of scan lines is now reduced, not only the peak temperature is reduced but also the heating interval is shorter than the limiting value as the percentage overlap is decreased.

Understanding the influence of scan geometry (L-W aspect ratio), percent overlapping (ϕ) and number of scan lines (N), on the raster-scan surface processing provides a method to tailor the surface peak temperature and heating interval as well as

the heating and cooling rates. This in turns affects the solidification or sintering conditions of the process and therefore the mechanical properties of the parts obtained.

References

[1] C.R. Deckard, "Method and apparatus for producing part by selective sintering", US Patent 4863538 (September 1989)

[2] S. Das, "Direct selective laser sintering of high performance metals : machine design, process development and process control", Ph.D. Dissertation Thesis, The University of Texas at Austin, December 1998

[3] W.M. Steen, Laser Material Processing, 2nd edition, (Springer Verlag 1993)

[4] J. Powell, P.S. Henry and W.M. Steen, "Laser Cladding with Preplaced powder: Analysis of thermal cycling and dilution effects", Surface Engineering, 4 1988, 141-149.

[5] Conde, R. Colaco, R. Vilar, J. de Damborenea, "Corrosion behavior of steels after laser surface melting", Materials & Design 21 (2000) 441-445

[6] H.S. Carls and J.C. Jaegger, Conduction of Heat in Solids, (Oxford 1996)

[7] J. A. Ramos Grez, "Surface modification of ceramic and metallic alloy substrates by laser raster-scanning", Ph.D. Dissertation Thesis, The University of Texas at Austin, August 2003